

Structural and Conformational Dynamics of Self-Assembling Bioactive β -Sheet Peptide Nanostructures Decorated with Multivalent RNA-Binding Peptides

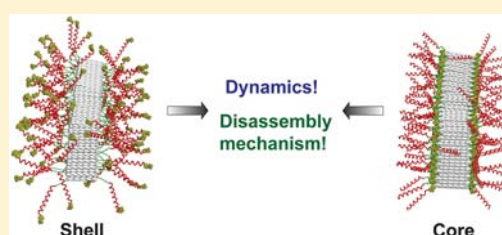
Sanghun Han,[†] Donghun Kim,[‡] So-hee Han,[†] Nam Hee Kim,[‡] Sun Hee Kim,^{*,‡} and Yong-beom Lim^{*,†}

[†]Translational Research Center for Protein Function Control and Department of Materials Science & Engineering, Yonsei University, Seoul 120-749, Korea

[‡]Division of Materials Science, Korea Basic Science Institute (KBSI), Daejeon 305-333, Korea

S Supporting Information

ABSTRACT: Understanding the dynamic behavior of nanostructural systems is important during the development of controllable and tailor-made nanomaterials. This is particularly true for nanostructures that are intended for biological applications because biomolecules are usually highly dynamic and responsive to external stimuli. In this Article, we investigated the structural and conformational dynamics of self-assembling bioactive β -sheet peptide nanostructures using electron paramagnetic resonance (EPR) spectroscopy. The model peptide nanostructures are characterized by the cross- β spine of β -ribbon fibers and multiple RNA-binding bioactive peptides that constitute the shell of the nanostructures. We found first, that bioactive peptides at the shell of β -ribbon nanostructure have a mobility similar to that of an isolated monomeric peptide. Second, the periphery of the cross- β spine is more immobile than the distal part of surface-displayed bioactive peptides. Third, the rotational dynamics of short and long fibrils are similar; that is, the mobility is largely independent of the extent of aggregation. Fourth, peptides that constitute the shell are affected first by the external environment at the initial stage. The cross- β spine resists its external environment to a certain extent and abruptly disintegrates when the perturbation reaches a certain degree. Our results provide an overall picture of β -sheet peptide nanostructure dynamics, which should be useful in the development of dynamic self-assembled peptide nanostructures.



INTRODUCTION

Self-assembled peptide nanostructures (SPNs) have great potential as promising biomaterials.^{1–4} Unlike proteins that consist of very long polypeptide chains with hundreds or more amino acids, SPNs are composed of peptides, that is, small fragments of proteins typically with less than 50 amino acids in size. Typically, hundreds or more than thousands of peptide building block molecules aggregate to form SPNs, resulting in the formation of high molecular weight aggregates. Therefore, despite their marked difference in their building block size (peptides vs very long polypeptides), the sizes of SPNs are comparable to or occasionally larger than those of proteins due to the process of bottom-up self-assembly. Research, even though still significantly primitive when compared to natural proteins, is in progress to devise SPNs that can mimic or displace the diverse biological functions of natural proteins, possibly with enhanced properties or with functions that are unprecedented in nature.^{5–10}

The self-assembly process is governed by various non-covalent interactions that force the building blocks into the formation of stable, low energy state aggregates. Many inter- and intramolecular noncovalent interactions function in concert during the formation of SPNs. Currently, the primary driving forces for self-assembly used to fabricate SPNs include nonspecific hydrophobic interactions, coiled-coil α -helical

bundle formation, β -sheet formation, and the combination of multiple different interactions.^{6,11–14} Among them, β -sheet-mediated SPN formation is gaining interest due to its potential to fabricate useful biomaterials as well as its relationship to amyloidogenic disease and protein misfolding.^{4,15–18} From a “materials perspective”, β -sheet-based SPNs can be used in the manufacture of nanostructures with high mechanical properties similar to spider thread and silk. In addition, β -sheet peptide building blocks with two dissimilar segments (block copolypeptides) can be used to make SPNs with multivalently displayed bioactive ligands on their surface.^{5,19–21} From an “amyloidogenic disease perspective”, understanding the mechanism of protein aggregation and pathogenesis is fundamental to devising therapeutics for this intractable disease.

Commonly used techniques for the analyses of nanostructural materials, such as SPNs, include transmission electron microscopy (TEM), circular dichroism (CD) spectroscopy, infrared (IR) spectroscopy, and dynamic light scattering (DLS). These tools are useful in acquiring information regarding nanostructural morphology, the molecular conformation of building blocks within the nanostructures, and size; however, these methods are of limited use for

Received: July 30, 2012

Published: August 31, 2012

observing structural and conformational dynamics of the nanostructural system. Thus, understanding the dynamics of SPNs should provide new information about the nanostructural peptide assembly system and further insight into the development of tailor-made SPNs.

EPR spectroscopy is a robust technique for studying the dynamic behavior of a system. EPR has been used to probe the structural and local dynamics of macromolecules and nanostructures, including proteins, DNAs, RNAs, polymers, dendrimers, carbon nanotubes, and gold nanoparticles.^{22–29} Among the many available EPR techniques, site-directed spin labeling (SDSL) is used to monitor the behavior of a stable nitroxide radical covalently attached at specific locations within a macromolecule.^{30,31} The obtained parameters, such as the internitroxide distances and descriptions of the rotational motion of a nitroxide, provide unique information on the features near the labeling site.

In the present work, we investigate the structural and conformational dynamics of a model RNA-binding^{32,33} bioactive β -sheet SPN system, combining SDSL with EPR spectroscopy.³⁴ Our ongoing research program has been focused on the controlled self-assembly of β -sheet block copolypeptide systems, which could lead to the development of peptide-based biologically applicable nanomaterials. Previous studies by our groups and others have provided important insight into the overall structure of β -sheet block copolypeptide assemblies and the molecular conformation of individual peptide building blocks; however, little is known about the dynamics of the assembly system. To our knowledge, this report is the first to study the dynamic behavior of β -sheet block copolypeptide SPNs using EPR spectroscopy.

RESULTS AND DISCUSSION

Design and Self-Assembly of β -Sheet Block Copolypeptide. Typical bioactive β -ribbon (β -sheet sandwich) nanostructures consist of a bioactive (usually hydrophilic and charged) peptide shell and an internal bilayered β -ribbon core (Figure 1e).^{3,19,29,31,35} The design strategy for the model bioactive β -ribbons used in this study is as follows. The peptide building blocks consist of two functionally different segments: a β -sheet forming segment and a bioactive peptide segment. The self-assembling β -sheet segments are primarily composed of alternating hydrophobic (tryptophan), positively charged (lysine), hydrophobic (tryptophan), and negatively charged (glutamic acid) amino acids, which have been shown to promote the formation of an antiparallel β -sheet structure (Figure 1a).^{7,20,30,32} Glutamine residues are placed at both ends of the segment to further stabilize the β strands. Glutamine residues are found in many amyloidogenic peptide sequences and are believed to strongly interact with each other, presumably via hydrophobic and complementary hydrogen-bonding interactions.³⁶ The bioactive segment is the peptide derived from the arginine-rich motif (ARM) of the HIV-1 Rev protein. Rev is an essential viral protein important in the nucleocytoplasmic export of viral RNA.³⁷ Rev ARM as an isolated peptide has been shown to tightly and specifically bind to Rev response element (RRE) mRNA of the virus in an α -helical conformation (Figure 1c).^{38,39} RRE is a large RNA structure (~350 nt) with multiple stem-loops, among which stem-loop IIB (~35 nt) is responsible for the initial and high-affinity binding.⁴⁰ Following the initial high-affinity binding to the IIB site, multiple Rev proteins oligomerize along full-length RRE by protein–RNA and protein–protein interactions.^{41,42}

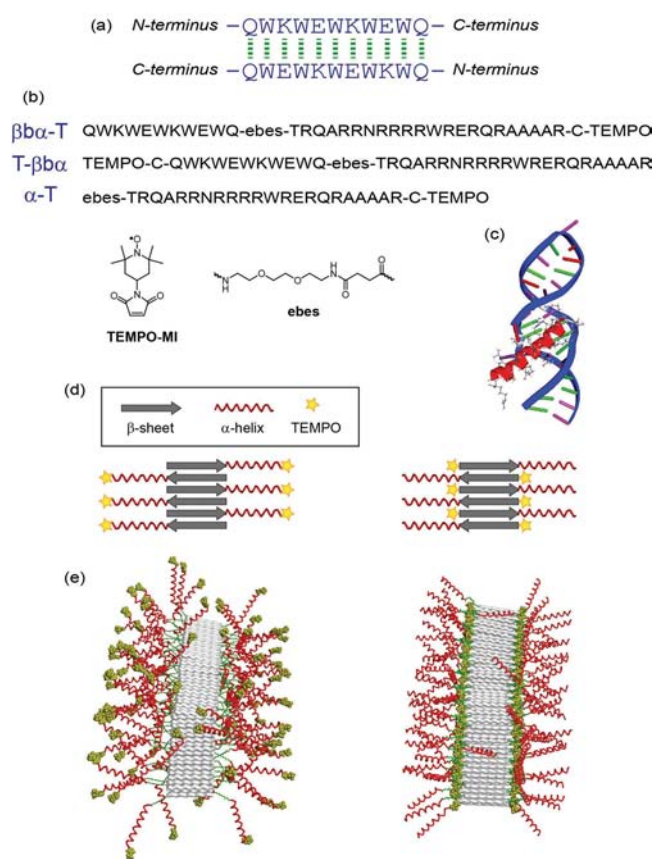


Figure 1. (a) Antiparallel β -sheet formation by the designed β -sheet segment. (b) Peptide sequences and SDSL with TEMPO. Sequence for a β -sheet segment, QWKWEWKWEWQ; a Rev ARM segment, TRQARRNRRRRWRERQRAAAAR. (c) NMR structure of the Rev ARM–RRE IIB RNA complex.⁴³ Protein Data Bank (www.rcsb.org) accession number 1ETF. (d) Schematic models of spin labeled peptide assemblies. (e) Molecular models for bioactive β -ribbon nanostructures. Left, β ba-T assembly; right, T- β ba assembly. Modeling was performed using Discovery Studio and Materials Studio (Accelrys).

Therefore, the overall configuration of the peptide building block is as follows: β -sheet forming segment–linker– α -helix forming bioactive segment (β -block- α , i.e., β ba).

In the proposed models of the bioactive β -ribbon assemblies (Figure 1d and 1e), the N-terminal and C-terminal regions appear to have quite contrasting mobilities. That is, the C-terminal part appears to be highly flexible, whereas the N-terminal part located at the core appears immobile. An alternative possibility is that the C-terminal region might not be as mobile as it appears due to the tight packing of Rev helices and intermolecular interactions; in addition, the N-terminal region might be unexpectedly flexible due to inefficient β -sheet formation or fraying at the end of the β -sheet.³¹ Understanding the dynamic properties of system is important because the function of many important biomolecules is derived from their dynamic properties and their ability to switch between different conformations. To address these fundamental and previously unanswered questions, we designed and synthesized block copolypeptides spin labeled with a 2,2,6,6-tetramethylpiperidine-1-oxyl (TEMPO) group at the C- or N-terminus (β ba-T, TEMPO at the C-terminus; T- β ba, TEMPO at the N-terminus). The conjugation reaction occurred between the maleimide group of TEMPO-MI and sulfhydryl moieties on cysteine residues of the peptide. Because

the TEMPO conjugation reaction was performed following the treatment of the peptide with a cleavage cocktail, a reduction in the spin label was prevented.

A variety of structural techniques were employed to probe the self-assembly behavior of the β -sheet block copolypeptides. Initially, the self-assembly behavior of the peptides was investigated by circular dichroism (CD) spectroscopy. As shown in Figure 2a and b, the CD spectra of both β β α -T and

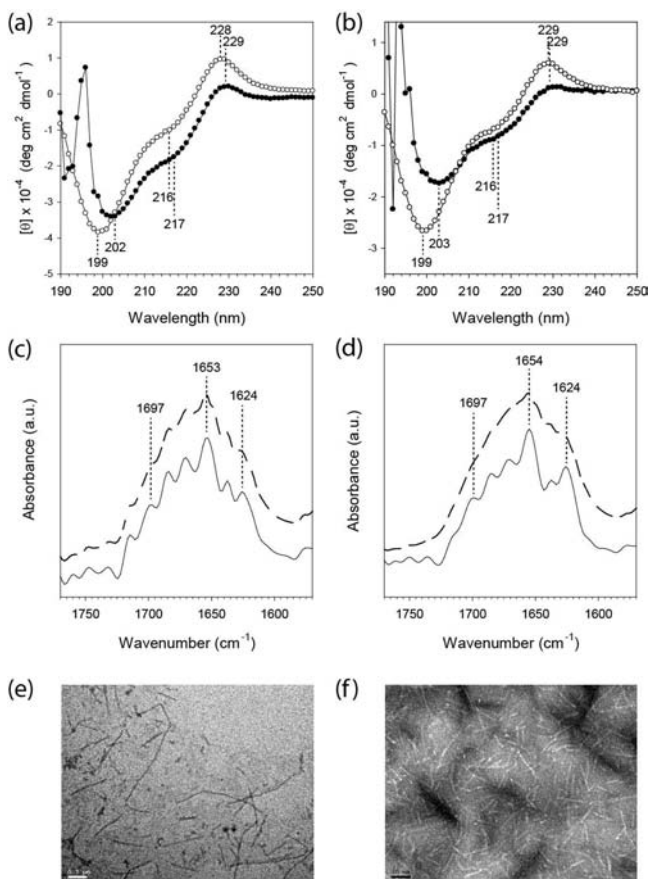


Figure 2. Characterization of the self-assembly process. CD spectra of (a) $\beta\beta\alpha$ -T and (b) T- $\beta\beta\alpha$ in pure water (○) and in 150 mM KF (●). All of the spectra were collected at 25 °C. [peptide] = 10 μ M. For the spectra collected in the presence of 150 mM KF, the wildly oscillating data at the lower wavelength range (less than 197–198 nm) are unreliable due to a significant increase in the high tension voltage and resulting detector saturation. FTIR spectra of (c) $\beta\beta\alpha$ -T and (d) T- $\beta\beta\alpha$. Original spectra (dashed line) and after Fourier self-deconvolution (solid line). Negative stain TEM images of (e) $\beta\beta\alpha$ -T and (f) T- $\beta\beta\alpha$.

T- $\beta\beta\alpha$ were very similar, suggesting a similar self-assembly behavior. In general, the spectra are characterized by two negative bands at 199–203 and 216–217 nm, and a positive band at 228–229 nm. The spectra were almost identical within the concentration range of 10–100 μ M. The negative band at 216–217 nm indicates that the building blocks form a β -sheet. Another negative band at 199–203 nm is likely attributable to a partially stabilized Rev ARM α -helical domain (vide infra). Although the Rev ARM domain binds RRE RNA in an α -helical conformation, it is difficult to form a fully stabilized helix at high temperature (here, room temperature) with the isolated peptide alone because helix formation is an enthalpy-driven process in which unfolding increases with temperature.⁴⁴

Although multiple Rev α -helical domains are located in a crowded environment due to the β -sheet-mediated self-assembly, such macromolecular crowding alone was shown to have a negligible influence on stabilizing the helical conformation, as evidenced by these CD data.

The positive band at 228–229 nm is an exciton-coupled band produced by the interaction between the aromatic tryptophan chromophores, indicating that Trp–Trp interactions help stabilize the β -sheet structure.^{45,46} With increasing ionic strength, the negative bands at 199 nm red-shifted to 202–203 nm, and increases in the strength of the β -sheet interaction (216–217 nm) were evident. It has been reported that β -sheet interactions can be strengthened by an increase in hydrophobic interactions at higher ionic strengths.^{19,47} The slightly red-shifted CD spectrum indicates a transition from a disordered random coil conformation to an ordered structure (here, a partially α -helical structure due to the high propensity of Rev ARM for helix formation).

FTIR spectroscopy studies corroborated the presence of β sheets (amide I bands at 1624 cm⁻¹) and α helices (1653–1654 cm⁻¹) in the peptide assemblies (Figure 2c,d). The weak bands at 1697 cm⁻¹ are characteristic of β strands in an antiparallel conformation.^{48,49} TEM micrographs show that both peptides form fibrillar nanostructures (Figure 2e,f). The nanostructures were shown to be discrete, suggesting the formation of a nanoribbon structure.^{19,50} The nanoribbons were heterogeneous in terms of the length population, which was ca. 50–500 nm. Nanoribbons from $\beta\beta\alpha$ -T appeared to be slightly longer than those from T- $\beta\beta\alpha$. In contrast to the relatively heterogeneous length population, the nanoribbon width was fairly homogeneous at 6–8 nm. In dimension, these are characteristics of fibrils of amyloidogenic β -sheet peptides.⁵¹ Considering the facts that interstrand distance of typical cross β -sheet structure is about 4.7 Å and the nanoribbon has a bilayered structure, the fibrillar nanoribbons should be composed of approximately 200–2000 or more peptide units.^{1,17} Taking all of these data together, structural models for the SPN of the copolypeptides can be established (Figure 1e). Both block copolypeptide building blocks self-assemble into antiparallel β -sheet nanoribbon structures, where slightly stabilized α helices of Rev ARM peptides surround the cross- β nanoribbon scaffold.

Interaction of Multivalent SPNs with an RNA Target.

This system is an example of a multivalent nanostructure in which bioactive peptides decorate a fibrillar β -ribbon scaffold. It has been shown that this type of multivalent β -sheet nanostructure can be developed as an efficient drug and gene delivery system.^{31,33} The system described here is unique in that multiple bioactive peptides at the surface of the nanostructure are involved in specific biomacromolecular interactions between RNA and the protein/peptide. The exploration of how this multivalent bioactive nanostructure interacts with RNA targets should yield valuable information on the development of multivalent inhibitors of RNA–protein interactions. In this specific example of an RNA–protein interaction, the binding of the Rev protein to RRE RNA is responsible for the nuclear export of viral RNA, which is essential for HIV-1 replication.⁴⁵ Therefore, inhibitors of Rev–RRE interactions can potentially be developed as AIDS drugs.⁵² Although the spatial orientation, linker length, and steric effect are not optimized, it should be interesting to investigate the RNA-binding characteristics of this multivalent system.^{53,54}

A fluorescence polarization (FP) assay was employed to quantitatively study the interaction of the Rev ARM peptide or β -ribbon with RRE RNA. Figure 3a shows the change in

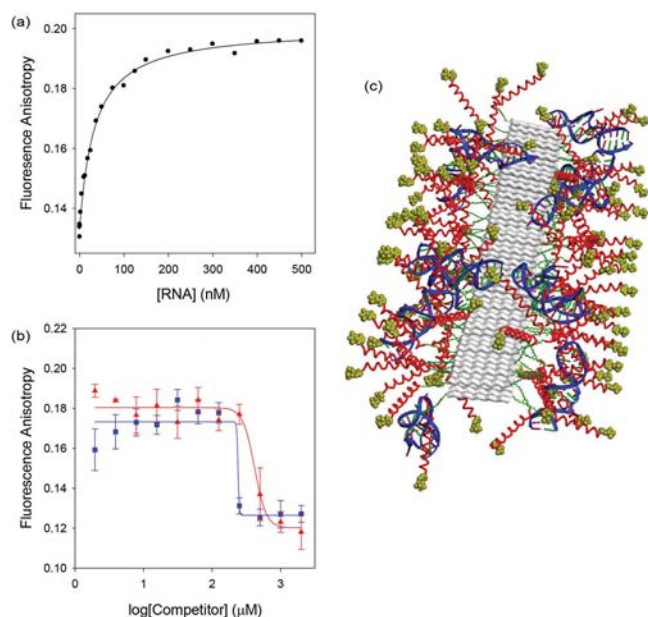


Figure 3. (a) Binding of a fluoresceinated-Rev ARM (FAM-Rev) peptide to RRE IIB RNA. (b) FP-based competition assay. Competitor: blue \blacksquare (α -T), red \blacktriangle ($\beta\alpha$ -T). (c) Model of a $\beta\alpha$ -T β -ribbon and IIB RNA complex.

fluorescence anisotropy of a fluoresceinated Rev ARM peptide (FAM-Rev) as a function of RRE IIB RNA concentration. The observed increase in anisotropy reflects the formation of a FAM-Rev/RRE IIB complex. Fitting the experimental data to a single-site binding model³² yielded a dissociation constant (K_d) of 33 nM (Figure 3a). An FP competition assay was then used to test whether the β -ribbon nanostructure could efficiently compete for RNA binding with the wild-type Rev ARM peptide. The assay was performed in the presence of a greater than 2-fold excess of RRE II RNA over the K_d to ensure complete peptide binding to RNA. As the concentration of competitors (α -T or $\beta\alpha$ -T) increased, there was a dose-dependent decrease in the fluorescence anisotropy, indicating the displacement of FAM-Rev off the RRE II RNA by specific RNA binding of the competitor. The competition experiments yielded EC_{50} values of 239 and 361 nM for the α -T and $\beta\alpha$ -T β -ribbon, respectively (Figure 3b). The relatively less effective competitiveness of the nanostructures ($\beta\alpha$ -T) relative to the single peptide molecule (α -T) can be explained by considering the steric effect. A consequence of self-assembly is the generation of a crowded environment for Rev ARM peptides, which inevitably hinders multiple large RNA molecules from binding to the β -ribbon (Figure 3c). Because of this steric effect, the competitiveness of the $\beta\alpha$ -T β -ribbon may in fact be better than that of α -T. There is an opportunity to explore this type of bioactive SPN as competitors/inhibitors of biomacromolecular interactions with potentially enhanced avidity, conformational stability, and multivalency. The inhibitory potency of bioactive SPNs should be improved with further studies. An in-depth investigation into this theme is beyond the scope of this Article and will be the subject of an ongoing study. One important result of this present study is that peptide-

displayed multivalent SPNs have potential competitiveness in biomacromolecular interactions between RNA and peptide.

EPR Characterization of Bioactive β -Ribbon Nanostructure Dynamics. Having established the structural and biological properties of SPNs, we subsequently scrutinized their dynamic properties by examining the rotational mobility of site-selectively attached nitroxide spin probes using continuous-wave EPR (CW-EPR) spectroscopy at the X-band (~ 9.6 GHz). EPR spectra of the spin-labeled SPNs shown in Figure 4

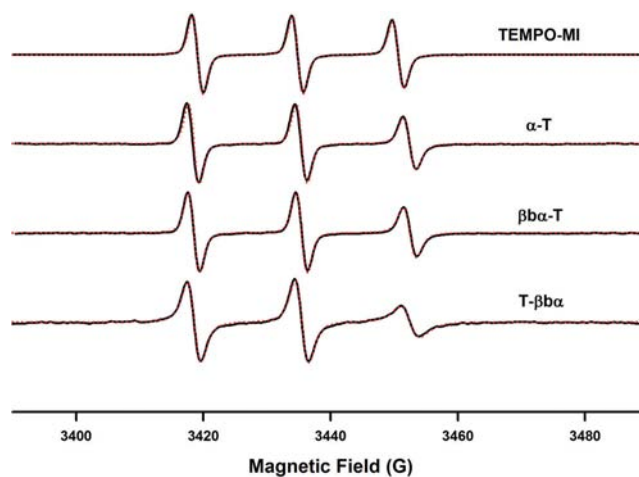


Figure 4. CW-EPR spectra of TEMPO-MI, α -T, $\beta\alpha$ -T, and T- $\beta\alpha$. The black solid lines and red dotted lines indicate the experimental data and their simulated spectra, respectively.

exhibited three hyperfine splittings from ^{14}N ($I = 1$) of a nitroxide probe. In addition, the line width and the rotational mobility were represented by the rotational correlation time, τ_c . X-band CW-EPR of nitroxides was sensitive to rotational correlation times between 10^{-10} and 10^{-6} s. The EPR spectrum of the free spin label, TEMPO-MI, at room temperature displayed three sharp lines that are typical of a nitroxide in the fast motional regime. The simulated spectrum displayed by the red dotted line is well reproduced by the experimental data with a τ_c of 70 ps.

To examine how the β -sheet segment affects the stability of the α -helix segment, we compared the EPR of α -T with that of $\beta\alpha$ -T. As shown in Figure 4, the EPR spectrum of α -T shows a decrease in the amplitude of the high-field line. The simulation of this EPR spectrum shows an increase of the rotational correlation time from 70 ps for the free nitroxide to 215 ps for α -T. The relatively high mobility of the labeled probe at the C-terminal end of the SPN confirmed that α -T is nonstructured and thus a highly flexible segment. In addition, the calculated rotational correlation time of $\beta\alpha$ -T (245 ps) was similar to that of the monomeric/free peptide (α -T), indicating that surface-displayed peptides on this nanostructure have mobility properties similar to those of free/isolated peptide. This finding should have important implications in the design of nanostructures and interpretation of the activities of bioactive nanostructures. One may assume that the mobility of peptides attached to SPNs may be much less than that of free peptides; however, the results of this study suggest that this is not the case.

In contrast, the spectrum of T- $\beta\alpha$ is quite different. The EPR spectrum of the label attached near the β -sheet showed a significant decrease in the amplitude and a broader line width of

the high field line, indicating a lower mobility than that of $\beta\beta\alpha$ -T. The simulated rotational correlation time of 730 ps increased by a factor of ~ 3 as compared to that of the distal part of the α -helix ($\beta\beta\alpha$ -T, 245 ps). (Table 1). This result is

Table 1. Dynamics of Bioactive β -Ribbon Nanostructures^a

| | TEMPO-MI | α -T | $\beta\beta\alpha$ -T | T- $\beta\beta\alpha$ |
|-------------|----------|------------------|-----------------------|-----------------------|
| pure water | | 215 ^b | 245 | 730 |
| KF (150 mM) | | 220 | 300 | 800 |
| DMSO | 70 | | | |

^a[peptide] = 100 μ M. ^bRotational correlation time (τ_c , ps).

consistent with the proposed model, which is based on the nanostructural characterization data (Figure 1e). Therefore, the results reveal that the region of the nanostructure adjacent to the cross- β core is more immobilized than the distal part of the nanostructure. Overall, the measured rotational correlation times of the SPNs were ranked as follows: τ (α -T) \approx τ ($\beta\beta\alpha$ -T) $<$ τ (T- $\beta\beta\alpha$). Because τ_c is inversely related to the mobility of the spin-label, this result clearly indicates a difference in the mobility of the spin labels at different sites on the SPNs.

We then examined the dependence of the mobility of the SPNs on the ionic strength of the solvents. Unexpectedly, the ionic strength dependence data revealed that the ionic strength has a negligible influence on the rotational correlation time of the spin-labels attached to different sites on the SPNs (Figure 5). We observed similar EPR spectra for $\beta\beta\alpha$ -T and T- $\beta\beta\alpha$ with

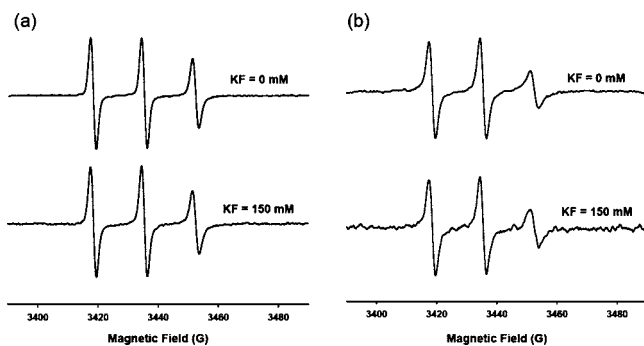


Figure 5. CW-EPR spectra of (a) $\beta\beta\alpha$ -T and (b) T- $\beta\beta\alpha$ in the absence (upper) and the presence (below) of 150 mM of potassium fluoride (KF).

and without 150 mM KF. A close examination of the simulating the spectra produced a similar rotational time (Table 1). These results contrast with the CD data, which showed a positive correlation between the ionic strength and the extent of β -sheet-mediated self-assembly (vide ante). It should be noted that the β -sheet had already formed in the absence of salt (KF), and KF merely increased the strength of the β -sheet interaction, which should have resulted in the formation of longer fibrils.^{19,40,47} That is, short (or oligomeric) fibrils had already formed in pure water, and longer and more mature fibrils formed at a higher ionic strength. Therefore, these combined results suggest that rotational dynamics for short and long fibrils are similar, and their local environments are not substantially different. This conclusion is reasonable considering that short fibrils may consist of at least more than dozens of peptide units, and contiguous peptide building blocks should exert the most influential effect on the overall dynamics.

By correlating the extent of secondary structural elements within nanostructures and the mobility of spin labels, we attempted to gain further insight into the structural dynamics of SPNs. As the concentration of 1,1,1,3,3,3-hexafluoro-2-propanol (HFIP) increased, noticeable transitions in the peptide conformation occurred (Figure 6a). HFIP is a strong β -breaker

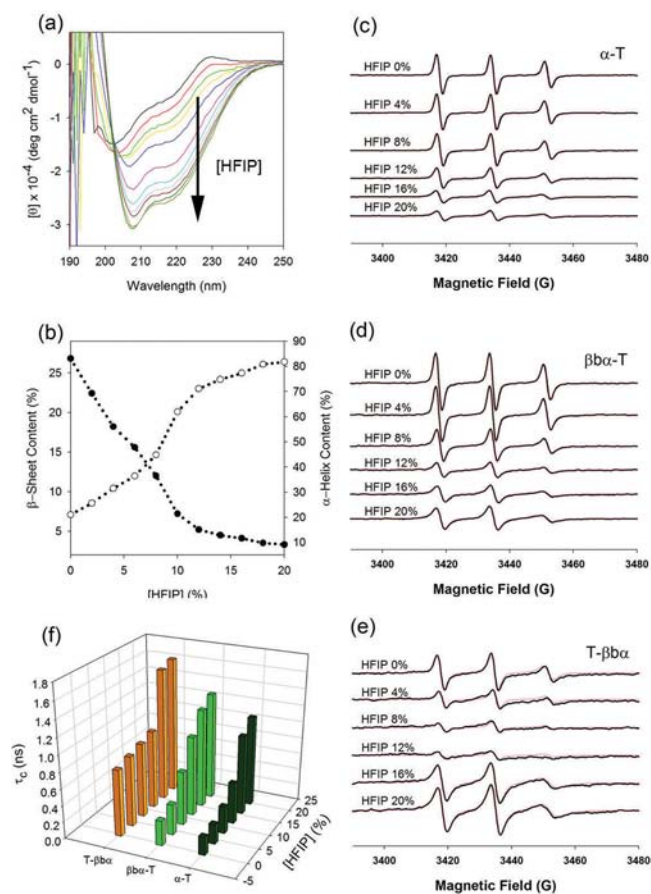


Figure 6. Effect of a destabilizing agent and implications in the disassembly mechanism of bioactive β -sheet SPNs. (a) Effect of HFIP on the secondary structure of T- $\beta\beta\alpha$ (10 μ M in 150 mM KF). (b) Deconvolution of CD spectra. O, α -helix content; \bullet , β -sheet content. CW-EPR spectra of the spin-labeled (c) α -T, (d) $\beta\beta\alpha$ -T, and (e) T- $\beta\beta\alpha$ with different concentrations of HFIP. The black solid lines and red dotted lines represent the experimental data and their simulated spectra, respectively. (f) The simulated values of the rotational correlation time for α -T, $\beta\beta\alpha$ -T, and T- $\beta\beta\alpha$ with different concentrations of HFIP. All of the spectra were collected at 298 K.

and is also known to stabilize α -helices.^{55,56} The deconvolution of the CD spectra shows that the β -sheet content decreased as the concentration of HFIP increased, while there was a simultaneous increase in α -helix content (Figure 6b). The deconvolution data show that abrupt changes in both the β -sheet and α -helix structures exist at an HFIP concentration range of 10–15%. It is likely that the self-assembled structure began to separate into individual peptide molecules within this concentration range. At the highest concentration of HFIP used in this study, the β -sheet content was approximately 0%, whereas the α -helix content was greater than 80%. Therefore, these data show that in the presence of a large amount of HFIP (here, 20%), not only was the Rev ARM potential α -helix domain stabilized, but the original β -sheet domain underwent a transition to an α -helix.

When the spin label itself was monitored by EPR, the increasing concentration of HFIP caused the spectral line shape of both α -T and $\beta\alpha$ -T, where the spin labels are attached to the potential Rev ARM α -helix, to become broader and the peak height to be decreased, which is consistent with a decrease in the average motion of the spin label with respect to its local environment (Figure 6c–f). These peptides shared similarity in that they showed gradual increases in τ_c and gradual decreases in amplitude, suggesting that the stability of the α -helix is enhanced in a stepwise fashion.

In contrast, the results for T- $\beta\alpha$ were quite different. There was an abrupt increase in the EPR amplitude at 16% [HFIP] (Figure 6e). A similar trend was also observed for τ_c . τ_c hardly changed up to [HFIP] 12%, although there was drastic change in τ_c when the HFIP concentration reached 16% (Figure 6f). In addition, there was an indication that the spectra of T- $\beta\alpha$ in the presence of 4–12% HFIP contained inhomogeneous features that could reflect an exchange between the mobile spin labels and the immobile population.

Taking all of these results into consideration, two conclusions can be drawn from the HFIP dependence experiment (Figure 7). First, gradual changes in τ_c and EPR

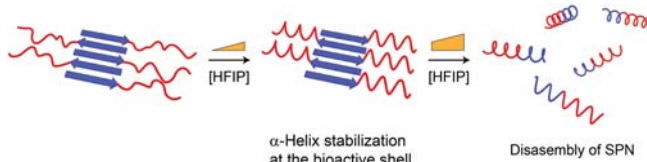


Figure 7. Model for the HFIP-induced discontinuous disassembly process.

signal amplitude from both α -T and $\beta\alpha$ -T reconfirm the notion that a surface-displayed peptide on the nanostructure has mobility properties similar to those of a free/isolated peptide (vide ante) in this type of block copolypeptide β -sheet assembly. Because the α -helix structure of the Rev ARM domain is stabilized with increasing HFIP concentration, the mobility decreases due to the restricted motion of the spin label. Second, the SPNs resist disassembly at HFIP concentration of up to 12%, and when [HFIP] reaches 16%, the SPN abruptly disassembles. That is, the shell domain is more easily affected by the external environment, whereas the β -sheet core domain resists the external environment to a certain extent. In addition, when the external force reaches a certain level, the SPN rapidly disassembles. On the basis of this discontinuous disassembly behavior, we may be able to obtain a glimpse of the disassembly behavior of block copolypeptide assemblies in a cellular environment. Molecular dynamic simulations have revealed the presence of a phase transition between the uncondensed state and the condensed state during the assembly of amyloid peptide.^{57,58} Thus, the results from this study indicate that a distinct phase transition also exists during the disassembly of amyloid-type peptides. Cooperative behavior of β -sheet self-assembly involving a dynamic interplay of multiple noncovalent interactions should be responsible for the existence of these distinct phase transitions.^{58,59}

CONCLUSIONS

In the present study, we successfully employed an EPR SDSL technique to probe the dynamic behavior of β -sheet-based bioactive SPNs. Our study revealed that the cross- β spine of a

β -ribbon fiber is more immobile than surface-displayed bioactive peptides, which is reasonable considering the structure of assemblies. Unexpectedly, the mobility of the surface-displayed bioactive peptides was almost similar to that of free peptides, and the mobility was largely independent of the extent of aggregation. This study also provided valuable insight on the disassembly mechanism of β -sheet-based bioactive SPNs, which was shown to be discontinuous. An understanding of the disassembly behavior should be informative in predicting the fate and stability of SPNs within an intracellular environment. Moreover, the disassembly behavior of this model β -sheet peptide should, in part, be related to that of β -amyloid peptides.

Polyvalent or multivalent interactions are frequently used in biology to enhance the affinity, avidity, and specificity of binding.^{11,22,60,61} Peptides, as epitopes or ligands, have been widely used as a miniaturized version of proteins. Extending beyond the capabilities of simple peptides, SPNs can be used as powerful platforms for constructing versatile, dynamic, and multivalent architectures. The key to the successful applications of SPNs is the ability to control their various physicochemical properties to meet the demands of dynamic biological conditions. Obtaining information on dynamic and structural properties of SPNs by EPR spectroscopy should be a valuable approach during the development of multivalent bioactive nanoarchitectures.

ASSOCIATED CONTENT

Supporting Information

Chemical structures of the peptides, MALDI-TOF MS spectra, EPR power dependence, and experimental procedures. This material is available free of charge via the Internet at <http://pubs.acs.org>.

AUTHOR INFORMATION

Corresponding Author

yblim@yonsei.ac.kr; shkim7@kbsi.re.kr

Notes

The authors declare no competing financial interest.

ACKNOWLEDGMENTS

This work was supported by the Seoul R&BD program (ST110029M0212351) and KBSI grant T32411.

REFERENCES

- Lim, Y. B.; Moon, K. S.; Lee, M. *Chem. Soc. Rev.* **2009**, *38*, 925–934.
- Woolfson, D. N.; Mahmoud, Z. N. *Chem. Soc. Rev.* **2010**, *39*, 3464–3479.
- Zelzer, M.; Ulijn, R. V. *Chem. Soc. Rev.* **2010**, *39*, 3351–3357.
- Cherny, I.; Gazit, E. *Angew. Chem., Int. Ed.* **2008**, *47*, 4062–4069.
- Baldwin, A. J.; Bader, R.; Christodoulou, J.; MacPhee, C. E.; Dobson, C. M.; Barker, P. D. *J. Am. Chem. Soc.* **2006**, *128*, 2162–2163.
- Hartgerink, J. D.; Beniash, E.; Stupp, S. I. *Science* **2001**, *294*, 1684–1688.
- Lim, Y. B.; Moon, K. S.; Lee, M. *Angew. Chem., Int. Ed.* **2009**, *48*, 1601–1605.
- Silva, G. A.; Czeisler, C.; Niece, K. L.; Beniash, E.; Harrington, D. A.; Kessler, J. A.; Stupp, S. I. *Science* **2004**, *303*, 1352–1355.
- Guler, M. O.; Stupp, S. I. *J. Am. Chem. Soc.* **2007**, *129*, 12082–12083.
- Choi, S. J.; Jeong, W. J.; Kim, T. H.; Lim, Y. B. *Soft Matter* **2011**, *7*, 1675–1677.

- (11) Apostolovic, B.; Danial, M.; Klok, H. A. *Chem. Soc. Rev.* **2010**, *39*, 3541–3575.
- (12) Lim, Y. B.; Lee, E.; Lee, M. *Angew. Chem., Int. Ed.* **2007**, *46*, 9011–9014.
- (13) Russell, L. E.; Fallas, J. A.; Hartgerink, J. D. *J. Am. Chem. Soc.* **2010**, *132*, 3242–3243.
- (14) Nagarkar, R. P.; Hule, R. A.; Pochan, D. J.; Schneider, J. P. *J. Am. Chem. Soc.* **2008**, *130*, 4466–4474.
- (15) Ghadiri, M. R.; Granja, J. R.; Milligan, R. A.; McRee, D. E.; Khazanovich, N. *Nature* **1993**, *366*, 324–327.
- (16) Lee, J.; Culyba, E. K.; Powers, E. T.; Kelly, J. W. *Nat. Chem. Biol.* **2011**, *7*, 602–609.
- (17) Hamley, I. W. *Angew. Chem., Int. Ed.* **2007**, *46*, 8128–8147.
- (18) Ni, R.; Childers, W. S.; Hardcastle, K. I.; Mehta, A. K.; Lynn, D. *G. Angew. Chem., Int. Ed.* **2012**, *51*, 6635–6638.
- (19) Lim, Y. B.; Lee, E.; Lee, M. *Angew. Chem., Int. Ed.* **2007**, *46*, 3475–3478.
- (20) Lim, Y. B.; Lee, E.; Yoon, Y. R.; Lee, M. S.; Lee, M. *Angew. Chem., Int. Ed.* **2008**, *47*, 4525–4528.
- (21) Lim, Y. B.; Kwon, O. J.; Lee, E.; Kim, P. H.; Yun, C. O.; Lee, M. *Org. Biomol. Chem.* **2008**, *6*, 1944–1948.
- (22) Zhang, X.; Lee, S. W.; Zhao, L.; Xia, T.; Qin, P. Z. *RNA* **2010**, *16*, 2474–2483.
- (23) Torbeev, V. Y.; Raghuraman, H.; Hamelberg, D.; Tonelli, M.; Westler, W. M.; Perozo, E.; Kent, S. B. *Proc. Natl. Acad. Sci. U.S.A.* **2011**, *108*, 20982–20987.
- (24) Ionita, P.; Volkov, A.; Jeschke, G.; Chechik, V. *Anal. Chem.* **2008**, *80*, 95–106.
- (25) Xia, Y.; Li, Y.; Burts, A. O.; Ottaviani, M. F.; Tirrell, D. A.; Johnson, J. A.; Turro, N. J.; Grubbs, R. H. *J. Am. Chem. Soc.* **2011**, *133*, 19953–19959.
- (26) Li, Q.; Fung, L. W. *Biochemistry* **2009**, *48*, 206–215.
- (27) Kirby, T. L.; Karim, C. B.; Thomas, D. D. *Biochemistry* **2004**, *43*, 5842–5852.
- (28) Junk, M. J.; Li, W.; Schluter, A. D.; Wegner, G.; Spiess, H. W.; Zhang, A.; Hinderberger, D. *Angew. Chem., Int. Ed.* **2010**, *49*, 5683–5687.
- (29) Lorenzi, M.; Puppo, C.; Lebrun, R.; Lignon, S.; Roubaud, V.; Martinho, M.; Mileo, E.; Tordo, P.; Marque, S. R.; Gontero, B.; Guigliarelli, B.; Belle, V. *Angew. Chem., Int. Ed.* **2011**, *50*, 9108–9111.
- (30) Hess, J. F.; Budamagunta, M. S.; Shipman, R. L.; FitzGerald, P. G.; Voss, J. C. *Biochemistry* **2006**, *45*, 11737–11743.
- (31) Kier, B. L.; Shu, L.; Eidenschink, L. A.; Andersen, N. H. *Proc. Natl. Acad. Sci. U.S.A.* **2010**, *107*, 10466–10471.
- (32) Cho, J. H.; Rando, R. R. *Biochemistry* **1999**, *38*, 8548–8554.
- (33) Kirk, S. R.; Luedtke, N. W.; Tor, Y. *J. Am. Chem. Soc.* **2000**, *122*, 980–981.
- (34) Stoll, S.; Schweiger, A. *J. Magn. Reson.* **2006**, *178*, 42–55.
- (35) Eckhardt, D.; Groenewolt, M.; Krause, E.; Borner, H. G. *Chem. Commun.* **2005**, 2814–2816.
- (36) Aggeli, A.; Nyrkova, I. A.; Bell, M.; Harding, R.; Carrick, L.; McLeish, T. C. B.; Semenov, A. N.; Boden, N. *Proc. Natl. Acad. Sci. U.S.A.* **2001**, *98*, 11857–11862.
- (37) Pollard, V. W.; Malim, M. H. *Annu. Rev. Microbiol.* **1998**, *52*, 491–532.
- (38) Tan, R.; Chen, L.; Buettner, J. A.; Hudson, D.; Frankel, A. D. *Cell* **1993**, *73*, 1031–1040.
- (39) Battiste, J. L.; Mao, H.; Rao, N. S.; Tan, R.; Muhandiram, D. R.; Kay, L. E.; Frankel, A. D.; Williamson, J. R. *Science* **1996**, *273*, 1547–1551.
- (40) Lockwood, N. A.; van Tankeren, R.; Mayo, K. H. *Biomacromolecules* **2002**, *3*, 1225–1232.
- (41) Jain, C.; Belasco, J. G. *Mol. Cell* **2001**, *7*, 603–614.
- (42) Daugherty, M. D.; Liu, B.; Frankel, A. D. *Nat. Struct. Mol. Biol.* **2010**, *17*, 1337–1342.
- (43) Battiste, J. L.; Mao, H. Y.; Rao, N. S.; Tan, R. Y.; Muhandiram, D. R.; Kay, L. E.; Frankel, A. D.; Williamson, J. R. *Science* **1996**, *273*, 1547–1551.
- (44) Marqusee, S.; Robbins, V. H.; Baldwin, R. L. *Proc. Natl. Acad. Sci. U.S.A.* **1989**, *86*, 5286–5290.
- (45) Cochran, A. G.; Skelton, N. J.; Starovasnik, M. A. *Proc. Natl. Acad. Sci. U.S.A.* **2001**, *98*, 5578–5583.
- (46) Grishina, I. B.; Woody, R. W. *Faraday Discuss.* **1994**, *99*, 245–262.
- (47) Lin, M. S.; Chen, L. Y.; Tsai, H. T.; Wang, S. S. S.; Chang, Y.; Higuchi, A.; Chen, W. Y. *Langmuir* **2008**, *24*, 5802–5808.
- (48) Matsuura, K.; Murasato, K.; Kimizuka, N. *J. Am. Chem. Soc.* **2005**, *127*, 10148–10149.
- (49) Ganesh, S.; Prakash, S.; Jayakumar, R. *Biopolymers* **2003**, *70*, 346–354.
- (50) Burkoth, T. S.; Benzinger, T. L. S.; Jones, D. N. M.; Hallenga, K.; Meredith, S. C.; Lynn, D. G. *J. Am. Chem. Soc.* **1998**, *120*, 7655–7656.
- (51) Janek, K.; Behlke, J.; Zipper, J.; Fabian, H.; Georgalis, Y.; Beyermann, M.; Bienert, M.; Krause, E. *Biochemistry* **1999**, *38*, 8246–8252.
- (52) Fineberg, K.; Fineberg, T.; Graessmann, A.; Luedtke, N. W.; Tor, Y.; Lixin, R.; Jans, D. A.; Loyter, A. *Biochemistry* **2003**, *42*, 2625–2633.
- (53) Kim, J. S.; Pabo, C. O. *Proc. Natl. Acad. Sci. U.S.A.* **1998**, *95*, 2812–2817.
- (54) Mammen, M.; Choi, S. K.; Whitesides, G. M. *Angew. Chem., Int. Ed.* **1998**, *37*, 2755–2794.
- (55) Wood, S. J.; Maleeff, B.; Hart, T.; Wetzel, R. *J. Mol. Biol.* **1996**, *256*, 870–877.
- (56) Hirota, N.; Mizuno, K.; Goto, Y. *Protein Sci.* **1997**, *6*, 416–421.
- (57) Cecchini, M.; Rao, F.; Seeber, M.; Caffisch, A. *J. Chem. Phys.* **2004**, *121*, 10748–10756.
- (58) Qi, X.; Hong, L.; Zhang, Y. *Biophys. J.* **2012**, *102*, 597–605.
- (59) Xu, W.; Zhang, C.; Derreumaux, P.; Graslund, A.; Morozova-Roche, L.; Mu, Y. *PLoS One* **2011**, *6*, e24329.
- (60) Mammen, M.; Choi, S. K.; Whitesides, G. M. *Angew. Chem., Int. Ed.* **1998**, *37*, 2754–2794.
- (61) van Baal, I.; Malda, H.; Synowsky, S. A.; van Dongen, J. L.; Hackeng, T. M.; Merkx, M.; Meijer, E. W. *Angew. Chem., Int. Ed.* **2005**, *44*, 5052–5057.